Journal of Materials Processing Technology 244 (2017) 87–96

Contents lists available at ScienceDirect

Journal of Materials Processing Technology

journal homepage: www.elsevier.com/locate/jmatprotec

Determination of forming ability of high pressure die casting for Zr-based metallic glass

L.H. Liu [a], J. Ma [b], C.Y. Yu [c], X.S. Huang [a], L.J. He [d], L.C. Zhang [e], P.J. Li [a,*], Z.Y. Liu [b,*]

[a] Department of Mechanical Engineering, Tsinghua University, Beijing 100084, China
[b] Guangdong Provincial Key Laboratory of Micro/Nano Optomechatronics Engineering, College of Mechatronics and Control Engineering, Shenzhen University, Shenzhen 518060, China
[c] College of Physics and Energy, Shenzhen University, Shenzhen 518060, China
[d] Department of Aerospace Engineering, Tsinghua University, Beijing 100084, China
[e] School of Engineering, Edith Cowan University, 270 Joondalup Drive, Joondalup, Perth, WA 6027, Australia

ARTICLE INFO

Article history:
Received 28 November 2016
Received in revised form 13 January 2017
Accepted 16 January 2017
Available online 19 January 2017

Keywords:
Bulk metallic glass
High pressure die casting
Critical casting sizes
Pressure

ABSTRACT

Large-sized industrial grade $Zr_{55}Cu_{30}Ni_5Al_{10}$ bulk metallic glass (BMG) was fabricated by a two-step arc-melting process and adding a trace of rare earth yttrium elements. A model to calculate critical cooling rate for forming BMG was established by considering the effect of pressure. Based on the model, the most important indicator, namely the critical size of forming BMG, for design and fabrication of BMG components by high pressure die casting (HPDC) is determined in consideration of different processing parameters, including the pressure and casting temperature. Theoretical calculation and numerical simulation indicated that increasing applied pressure during casting suppresses the nucleation of crystal nuclei but has little effect on the growth of nuclei at a deep supercooled temperature, thereby decreasing critical cooling rate and thus increase critical size. An increasing casting temperature would reduce critical size caused by more heat to dissipate. The critical size of the optimized $Zr_{55}Cu_{30}Ni_5Al_{10}$ BMG cast by using steel mold is determined to be about 4–7 mm under different HPDC parameters. Our study reveals that the forming ability of HPDC is large enough for fabricating low cost Zr-based BMGs with suitable size for applications.

1. Introduction

Among all bulk metallic glasses (BMGs), multicomponent zirconium (Zr) based alloys have superior glass forming ability (GFA) and can form into bulk form with critical dimension up to several centimeters by copper mold casting (Inoue and Takeuchi, 2011). Such sizes are big enough for applications as a structural material in many fields, such as sporting goods, ornamental parts and consumer electronics (Telford, 2004). However, large-scale industrialization application is still facing challenges, including the high cost of raw materials and absence of equipment that can be used to fabricate BMG parts with complex shapes in large-scale. Therefore, intensive endeavor has been made on above two fields in the past decades. With regard to lowering the price for BMGs, Jiang et al. (2005) founded that low-cost Zr-based BMGs can be prepared with a low purity sponge zirconium by introducing a small amount of rare earth element. Cheng et al. (2013) provided an innovative approach to fabricate low-cost Zr-based BMG composites by precipitating crystal Zr in melt to alleviate the detrimental effect of oxygen impurities. Regarding the forming methods, it was reported by Inoue et al. (2015) that many approaches, such as thermoplastic forming and selective laser melting, have been developed in the past years. However, a major drawback in using these techniques to produce BMGs with bigger and complex parts is either too short processing time or inevitable crystallization in the prepared sample. High pressure die casting (HPDC), as a metal casting process in real industries, is widely used to produce aluminum, magnesium, and copper alloys components by forcing molten metals under high pressure into a mold at high velocity. In recent years, various endeavors have been made to adopt HPDC to fabricate BMG parts with complex shape for applications, due to its characteristics of near net shape forming and high production efficiency. Heinrich et al. (2012) reported that $Zr_{58.5}Cu_{15.6}Ni_{12.8}Al1_{0.3}Nb_{2.8}$ BMG with size of 5 mm can be prepared by a horizontal vacuum cold-chamber die casting process. Ramasamy et al. (2016) found Fe-based bulk metallic glass key-shaped specimens can be fabricated by HPDC under Ar atmosphere. However, systematic study on the fabrication ability of HPDC for a certain composition is still absent.

As one of the most important indicators of the fabrication ability for a BMG or process method, the critical size has been stud-

* Corresponding authors.
E-mail addresses: lipj@mail.tsinghua.edu.cn (P.J. Li), zyliu@szu.edu.cn (Z.Y. Liu).

http://dx.doi.org/10.1016/j.jmatprotec.2017.01.015
0924-0136/

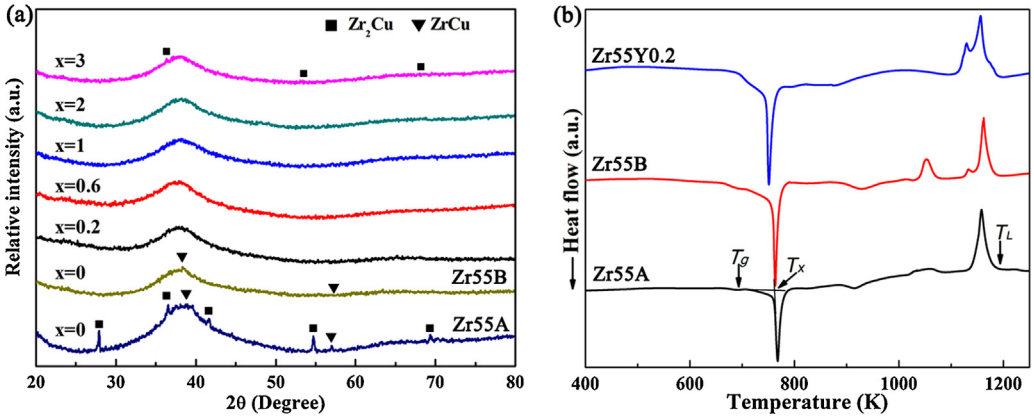

Fig. 1. (a) XRD patterns of the industrial grade $Zr_{55}Cu_{30}Ni_5Al_{10}$ alloys prepared by adding different content of Y element. (b) DSC curves of the as-cast alloy for different process.

ied extensively, and there exist a large number of data about the critical casting size of copper mold cast BMGs, such as 30 mm for $Zr_{55}Cu_{30}Ni_5Al_{10}$ BMG (Yokoyama et al., 2007), 10 mm for $Cu_{46}Zr_{42}Al_7Y_5$ BMG, and 10 mm for $Ti_{40}Zr_{26}Be_{28}Fe_6$ BMG, etc (Qiao et al., 2016). However, these data provide little guidance to evaluate fabrication ability or glass forming ability by HPDC, because the casting conditions in HPDC are substantially different from those for traditional copper mold casting in laboratory scale. For instance, the mold for HPDC is usually made of H13 steel in the consideration of high-temperature strength and durability. The steel mold has different thermal conductive properties compared to copper mold, thus leading to a significant difference in cooling capacity during casting. To predict the critical size of BMG by HPDC, one can start by comparing cooling rate during HPDC with the critical cooling rate (R_c) of BMG. Yet, the R_c of BMG fabricated by die casting cannot be precisely estimated using the present methods, such as the most common approach proposed by Uhlmann (1972); which was based on the theories of homogeneous nucleation and of crystal growth but without consideration of pressure.

In this work, low cost $Zr_{55}Cu_{30}Ni_5Al_{10}$ BMG was fabricated by a two-step arc-melting process by using industrial grade raw materials and adding a trace of rare earth yttrium elements. Uhlmann's model was modified to estimate the R_c of BMG farbricated under different pressures. By comparing the R_c and the cooling process of the Zr-based BMG castings with different diameters obtained by numerical simulations, the critical size of the Zr-based BMG by die casting under different pressure and casting temperature was determined to be 4–7 mm. Besides, it was found that a high pressure in HPDC increases the critical size but with the increment extent up to 1 mm, and the thermal conductivity of mold plays a great role in determining the critical size of BMGs. Therefore, it is expected the obtained results can providea guideline for designing and fabricating Zr-based BMG parts by HPDC for the industrial applications.

2. Experimental

Low purity sponge zirconium with a purity of 99.4% instead of high purity Zr was used to fabricate the low cost BMG for HPDC. The purity of the other elements Cu, Ni, Al and Y is 99.9%, 99.9%, 99.9%, and 99.9%, respectively. Ingots with nominal composition of $(Zr_{55}Cu_{30}Ni_5Al_{10})_{100-x}Y_x$ (x = 0, 0.2, 0.6, 1–3; at.%) were prepared by a two-step arc-melting process in an arc furnace. Firstly, sponge zirconium was arc-melted into an ingot, and then, mixtures of the as-melted Zr ingot with other constituent elements were melted in a Ti-gettered high purity argon atmosphere. Each ingot was re-melted at least four times to ensure chemical homogeneity. Afterwards, samples in cylinder of 5 mm in diameter and 70 mm long were produced by suction casting the melt into a copper mold. For comparison, a $Zr_{55}Cu_{30}Ni_5Al_{10}$ sample was directly melted by mixtures of the sponge zirconium with other constituent elements. In this work, the sample fabricated directly by mixtures of the sponge zirconium with other constituent elements was indicated as "Zr55A", the sample prepared by two-step arc-melting process was denoted as "Zr55B", and the samples with different yttrium contents were presented as "Zr55Yx", where "x" is the content of yttrium.

In order to determine the critical size of the optimized $Zr_{55}Cu_{30}Ni_5Al_{10}$ BMG by HPDC, firstly, a model, based on Uhlmann's method, was developed by taking pressure effect into account. Secondly, based on the above model, time-temperature-transformation (TTT) curve and continuous cooling transformation (CCT) curves were established, and from which the critical cooling rates of Zr-based BMGs under different pressures were estimated. The thermodynamics parameters in the model, such as melting point, freezing point and enthalpy of melting for the optimized BMG, were determined through differential scanning calorimetry (DSC) experiments. Finally, the cooling rates of castings with different diameters by HPDC were calculated by numerical simulations by the commercial software ProCAST. The critical size of BMG under different pressures and at casting temperatures was determined by comparing the simulated cooling rate and the calculated critical cooling rate.

The glassy nature of bulk samples was examined by the X-ray diffraction (XRD, Brucker Advance D8) technique with Cu Kα radiation. Thermal analysis was performed using differential scanning calorimetry (DSC, Perkin Elmer STA8000 and DSC8000) with a flow of purified argon gas at a heating rate of 20 K/min. Fracture surface is observed by a Philips XL-30 FEG scanning electron microscope. In order to evaluate the mechanical properties of the as-fabricated bulk alloys, cylindrical specimens of 5 mm in diameter and 10 mm in length were tested in a universal testing machine (MTS testing system) under quasi static loading at a strain rate of $5\times10^{-4}\ s^{-1}$, and a small strain gauge was used to calibrate and measure the strain during loading.

3. Results and discussion

3.1. Optimization of industrial grade BMGs

Fig. 1a displays XRD patterns of industrial grade $Zr_{55}Cu_{30}Ni_5Al_{10}$ alloys prepared by adding different content of Y. The $Zr_{55}Cu_{30}Ni_5Al_{10}$ alloy fabricated directly by all of low purity raw materials (denoted as Zr55A) cannot form a completely amor-

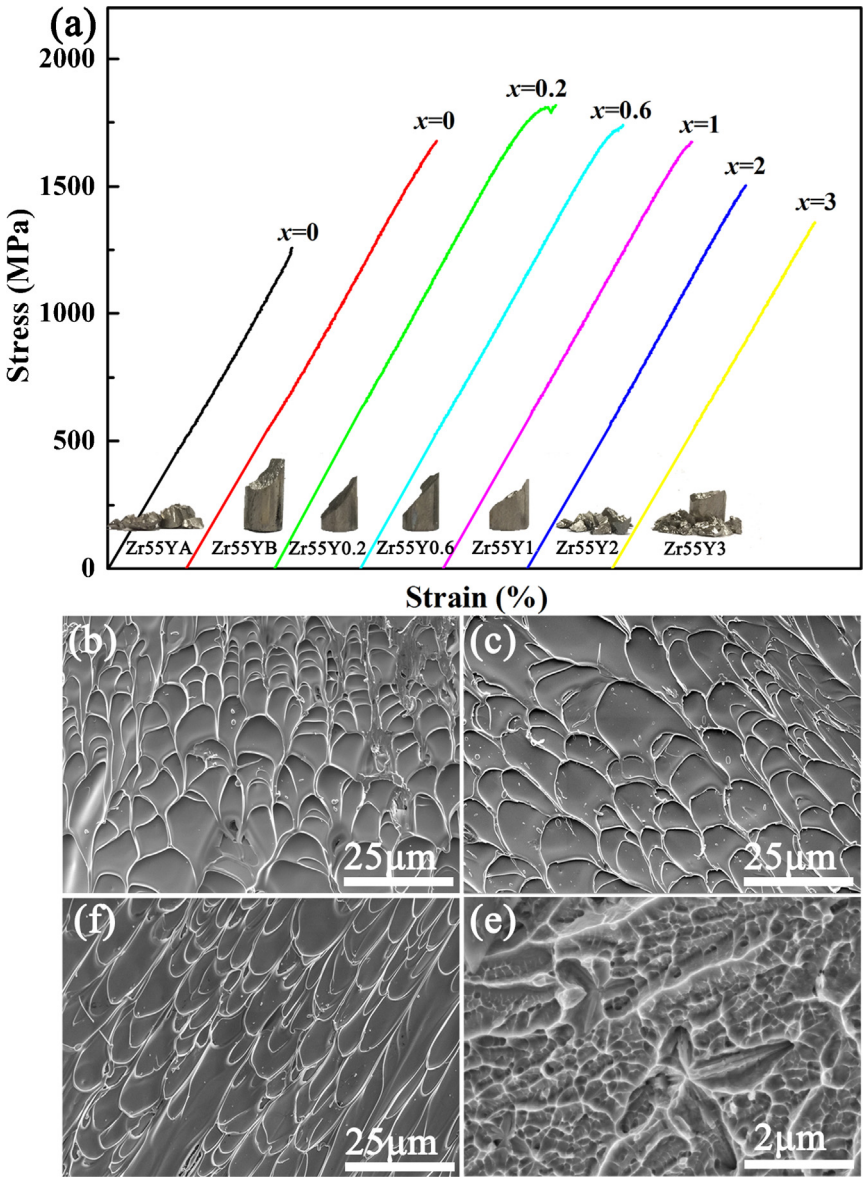

Fig. 2. (a) Compressive stress-strain curves of the industrial grade $Zr_{55}Cu_{30}Ni_5Al_{10}$ alloys prepared by adding different content of Y element. The insets are the macroscopic fracture patterns of the compressive specimens; SEM of fracture surface for different samples: (b) Zr55B, (c) Zr55Y0.2, (d) Zr55Y1, (f) Zr55Y3.

phous structure, in which a lot of crystalline phases, such as Zr_2Cu and ZrCu phases, are found in the as-cast alloy (Fig. 1a). While for the $Zr_{55}Cu_{30}Ni_5Al_{10}$ alloy fabricated by the two-step arc-melting process (indicated as Zr55B), only several tiny diffraction peaks superimposed on the diffuse halo are visible, indicating that the sample consists primarily of amorphous phase with a small amount of crystalline ZrCu phase. The critical size (less 5 mm) for BMG by using low purity raw materials here is far smaller than 25 mm of BMG by using high purity zirconium by Yokoyama et al. (2007), it is ascribed to the impurities in sponge zirconium can act as nuclci-formation sites during solidification, thus decreasing the GFA.By adding the rare earth element Y, XRD patterns in Fig. 1a show that broad humps can be seen in all of $(Zr_{55}Cu_{30}Ni_5Al_{10})_{100-X}Y_X$ (x = 0, 0.2, 0.6, 1–3) alloys (presented as Zr55Yx, where x = 0.2, 0.6, 1–3), but a few "spikes" can be detected in the pattern of Zr55Y3. This indicates that the GFA can be improved by adding rare earth element, but excess Y (x = 3) would deteriorate GFA. This can be explained based on the thermodynamics. Deng et al. (2015) reported that the values of the enthalpy of mixing of the Zr-O, Cu-O, Y-O is about −1108.2 kJ/mol −157.3 kJ/mol and −2000.3 kJ/mol, respectively, and the enthalpy of mixing of ZrO_2, CuO, CuO_2, Ni_2O_3, Al_2O_3 and Y_2O_3 is −1100.8, −157.3, −168.6, −489.5, −1675.7 and −1905.3 kJ/mol (Hu et al., 2014), respectively, showing that the Y has a stronger affinity with oxygen atoms compared with other alloy elements. Hence, it is easier for Y bonds with oxygen to form oxide Y_2O_3, which would significantly reduce the residual amount of dissolved oxygen available for forming ZrO_2. Jiang et al. (2005) shows the ZrO_2 can act as a nucleus to promote the nucleation and crystallization, while yttrium oxide cannot be the heterogeneous nucleation sites due to crystallographic structures, sizes dispersion and wetting behavior between solid/liquid interfaces. Therefore, the GFA of industrial grade $Zr_{55}Cu_{30}Ni_5Al_{10}$ alloy was improved by alleviation of the harmful effect of oxygen, while excess yttrium would form compound with other elements, thus decrease the GFA of $Zr_{55}Cu_{30}Ni_5Al_{10}$ alloy.

Fig. 1b displays DSC curves of the as-cast alloy sample Zr55A, Zr55B, and Zr55Y0.2. The relative volume fraction of amorphous phase V_r for $Zr_{55}Cu_{30}Ni_5Al_{10}$ alloy displays a signification increase from 78% to 96% by the two-step arc-melting process, then a full amorphous structure obtained for the Zr55BY0.2 by adding 0.2% Y

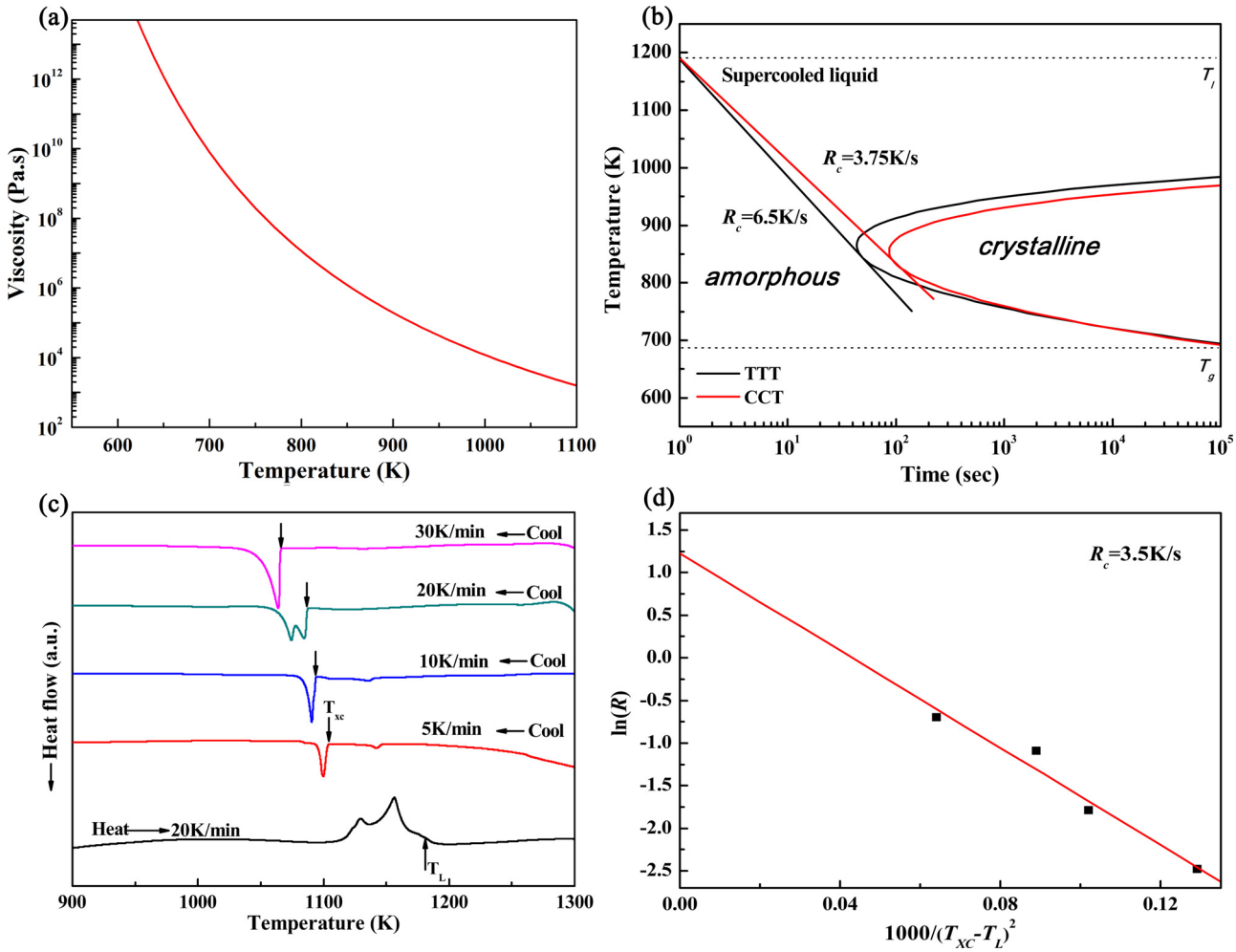

Fig. 3. (a) Viscosity of $Zr_{55}Cu_{30}Al_{10}Ni_5$ bulk metallic glasses as a function of temperature, (b) R_c obtained by Uhlmann's model by using experimental viscosity, (c) DSC curves for $Zr_{55}Cu_{30}Al_{10}Ni_5$ alloy cooling with different rate, (d) R_c obtained by Barandiaran and Colmenero's method.

in the two-step processed alloy. It is consistent with XRD results. Although the industrial grade raw materials are used in the present alloy, the minimum content of element Y to form an amorphous structure is far less than that in the reported BMG by Zhang et al. (2000) by directly smelted by mixtures of the sponge zirconium with other constituent elements. It is mainly ascribed to purification effect for the sponge zirconium by the two-step arc-melting process in the present case. Detail mechanism would be discussed in other place.

Fig. 2a presents room-temperature uniaxial compressive engineering stress-strain curves of the cast alloy. Apparently, except for that the sample Zr55Y0.2 possesses a plasticity of 0.2%, no plasticity is found in other alloys. For the sample prepared by directly smelting by mixtures of sponge zirconium with other constituent elements, the alloy Zr55A displays strength of 1250 MPa, which is far lower than that of the Zr55B alloy fabricated by the two-step arc-melting process. But the strength of Zr55 B is still lower than that of $Zr_{55}Cu_{30}Ni_5Al_{10}$BMG by high pure raw material (i.e. 1830 MPa) (Inoue and Takeuchi, 2011). The strength exhibits the highest 1800 MPa for alloy Zr55Y0.2 with adding 0.2% of Y and decreases with increasing Y content. The insets display the macroscopic fracture patterns of the compressive specimens, showing a typical shear failure with fracture angles of about 45° specimens Zr55Y0.2, Zr55Y0.6 and Zr55Y1, and either part or complete brittle fracture for other alloys that contain some crystallized phases. Many studies, such as Jiang et al. (2005), have shown that only a few crystals would dramatically decrease the strength and plasticity of BMGs. The phenomenon of alloys which are not a complete amorphous structure and display low strength accompanied by brittle fracture is in agreement with the above results. Further SEM observations were carried out on the fracture surfaces (Fig. 2b–e), which display characteristic peak-to-peak dimple patterns. The size of dimple-like structures on fracture surface, which can be defined as average spacing between ridges of dimples surrounding the center of each dimple zone, is about 18, 20 and 15 μm for Zr55YB, Zr55Y0.2 and Zr55Y1, respectively. While the value for the Zr55Y3 with complete brittle fracture is only about 0.5 μm, only 1/40 of the shear fracture one. Yuan et al. (2012) found that dimple pattern size is associated with plasticity of the alloy, and BMG with larger plasticity displays a lager dimple pattern. The result further revealed that Zr55Y0.2 BMG possesses superior mechanical property to other BMGs. Further GFA of Zr55Y0.2 BMG is studied, and XRD pattern suggests that the Zr55Y0.2 with diameter of 9 mm can form a complete amorphous structure, indicating that the critical size of Zr55Y0.2 fabricated by copper mold suction casting is not less than 9 mm (XRD not shown here). Based on above results, it can be concluded that the Zr55Y0.2 is the most suitable composition for preparing the master alloy for HPDC.

3.2. Determination of critical cooling rate

3.2.1. Model

To determine the critical size of the alloy fabricated by HPDC, we should start with the critical cooling rate. There exist several

methods to estimate the R_c. The most common method is adopting the model by Uhlmann (1972) to construct a TTT curve, which defines the time required at any temperature to produce a particular volume fraction of crystallization, x, typically in the order of 10^{-6}. Each TTT curve has an extreme or nose due to the competition between the increase in driving force for crystallization and decrease in diffusion with increase undercooling. The R_c for glass formation is approximated by the linear cooling curve required just to touch the nose of each TTT curve. The time for a given volume fraction, x, to crystallize is shown by Davies et al. (1974):

$$t = \frac{9.32\eta}{kT}\left(\frac{a_0^9 x \exp(1.024/T_r^3\Delta T_r^2)}{\bar{N}_0 f^3\left[1-\exp(-(\Delta H_M^f \Delta T)/RT)\right]^3}\right)^{1/4} \quad (1)$$

where $\bar{N}_0$ is the number of single atom per unit volume; η is the viscosity and k is Boltzmann's constant; $\Delta T = T - T_m$ is the undercooling, T_m is the melting point, and T is the absolute temperature in K; ΔT_r and T_r are the relative undercooling and relative temperature, respectively; R is ideal gas constant; f is the fraction of sites on the interface where atoms may preferentially be added and removed; ΔH_M^f is the heat of fusion and a_0 is a molecular diameter.

The Uhlmann's model is based on the classical theory of nucleation, the nucleation and growth barriers of nuclei are only dependent upon temperature, and the pressure during solidification has not been taken into account. Apparently, the model cannot described accurately the solidification process of HPDC, because the molten alloy often sustains a high pressure up to several hundred MPa to improve the product quality and productivity. According to the classical nucleation theory, crystal nucleation frequency I and growth rate u are both affected by pressure through the activation energy. Therefore, it is essential to consider the pressure effect in the model in order to estimate more accurate R_c of the BMG under cooling condition of HPDC. It was reported that the activation energy for the formation of stable nuclei, ΔG^*, can be expressed by Turnbull (1965): $\Delta G^* = \frac{16\pi\sigma^3}{3(\Delta G)^2}$, where σ and ΔG are the interfacial energy and free energy difference between the nuclei and liquid phase, respectively. According to statement by Miller and Chadwick (1967), the interfacial energy σ is temperature-dependent, which can be written as, $\sigma = \frac{\alpha\Delta H_M^f}{(N_A V_M^2)^{1/3}} \cdot \frac{T}{T_m}$, where α is a crystallographic parameter, N_A is the Avogadro's constant, and V_M is molar volume. According to the Thompson's simplified equations (Johnson, 1986), ΔG approximately satisfies the equation, $\Delta G = \Delta H_M^f \frac{2T_r\Delta T_r}{1+T_r}$. 'It was found that the activation energy ΔG_p^* for the formation of stable nuclei under pressure can be expressed as (Wang et al., 2004):

$$\Delta G_p^* = \frac{16\pi\sigma^3}{3(\Delta G + P\Delta V)^2} \quad (2)$$

Herein, ΔV is the molar volume difference between the liquid and crystalline phases, and it decreases by about 1% after crystallization from amorphous phase, P is the applied pressure. Hence, the increment of nucleation energy caused by pressure effect is: $\Delta E_p^I = \Delta G_p^* - \Delta G^*$.

Besides, it is similar to the pressure effect on the activation energy for growth rate (Wang et al., 2004). The increment is:

$$\Delta E_p^U = P\Delta V \quad (3)$$

As we known, the pressure can also affect the undercooling of melt metal according to the Clapeyron-Clausius equation (Kang et al., 2000), $\Delta T/\Delta P = T(V_L - V_S)/\Delta H_M^f$, where, V_1 and V_s are the specific volumes of the liquid and solid phase, respectively. The relative undercooling under die casting pressure, ΔT_r^P, can be expressed as:

$$\Delta T_r^p = \frac{\Delta T - (e^{P(V_L - V_S)/\Delta H_M^f} - 1)T_{xc}}{T_m} \quad (4)$$

where T_{xc} is solidification temperature.

Considering above deductions together, a model of about the critical cooling rate considering the pressure effect during the solidification is established:

$$t = \frac{9.32\eta}{kT}\left(\frac{a_0^9 x \exp(1.024/T_r^3\Delta T_r^{P2} + \Delta E_p^I/kT)}{\bar{N}_0 f^3\left[1-\exp(-(\Delta H_M^f \Delta T_r^P + \Delta E_p^U)/RT)\right]^3}\right)^{1/4} \quad (5)$$

It should be note here the other parameters like the viscosity of supercool liquid is not considered in the modified model, this is mainly ascribed to the reasons as follows: on one hand, the present modified model is established based on the Uhlmann' method, which is from the classical theory of nucleation. Therefore, our modified model is mainly discussed the pressure effect on the nucleation and growth activation energy. On the other hand, the effect of pressure on the viscosity is rarely reported due to the difficulty in experiment. While the diffusion coefficient can be related with viscosity by the Stokes-Einstein equation, $\nu = kT/3\pi a_0^3\eta$. Wang et al. (2004) found that the effect of pressure on the diffusion activation energy, Q, can be ignored as the pressure is often below 0.3 GPa in actual production process for HPDC, thus have little effect on viscosity.

3.2.2. Parameters in the modified model

The temperature dependence of viscosity is a key parameter for constructing TTT curves. For supercooled liquid of Zr-based BMG-forming alloy, the viscosity follows the widely accepted Vogel-Fulcher's expression over the entire temperature range: $\eta(T) = A\exp\left(\frac{B}{T-T_0}\right)$, where A, B and T_0 are constants. The viscosity is always determined under various assumptions. For example, the viscosity of the BMG is 10^{12} Pa s at temperature of T_g; the viscosity of the cast Zr-based BMG is equal to the viscosity of pure Zr at its melting point, T_m, and so on (Hng et al., 1996). Virtually, the viscosity of supercooled liquid for the BMG is sensitive to temperature (Liu et al., 2015). The calculated critical cooling rates by using the viscosity obtained by this method always display a large fluctuation. For example, Hng et al. (1996) found the computed critical cooling rate of a $Zr_{66}Ni_{26}Al_8$ BMG changes from 0.81 K/s to 260 K/s by using the fitted viscosity obtained by using above different assumptions. Therefore, it is essential to obtain the viscosity-temperature fitted data based on experimental measurements in order to obtain a more realistic estimation of the critical cooling rate to predict critical size of Zr55Y0.2 metallic glass by HPDC. The viscosity of $Zr_{55}Cu_{30}Al_{10}Ni_5$ supercooled liquid has been measured by using a penetration viscometer under at different heating rates by Yamasaki et al. (2006). Comparing to the large fluctuation by above various assumptions, here it is assumed that effect of 0.2% yttrium on the viscosity of $Zr_{55}Cu_{30}Al_{10}Ni_5$ BMG can be ignored. Therefore, the viscosity used for calculating the TTT curve can be obtained by extrapolation method based on (Yamasaki et al., 2006), thus can be given as: $\ln\eta = -5.5 + 9425/(T-366)$, as shown in Fig. 3a.

For the other parameters in the developed model, the molecular diameter a_0, which is obtained from an atomic percent weighted for each alloy, is 0.2899 nm. The number of single molecules per unit volume $\bar{N}_0$ calculated by assuming ideal liquid mixing is 5.02×10^{28}. The melting temperature T_m and the heat of fusion ΔH_M^f, which is determined from DSC measurement by using the as-fabricated industrial grade Zr55Y0.2 BMG, are 1125 K

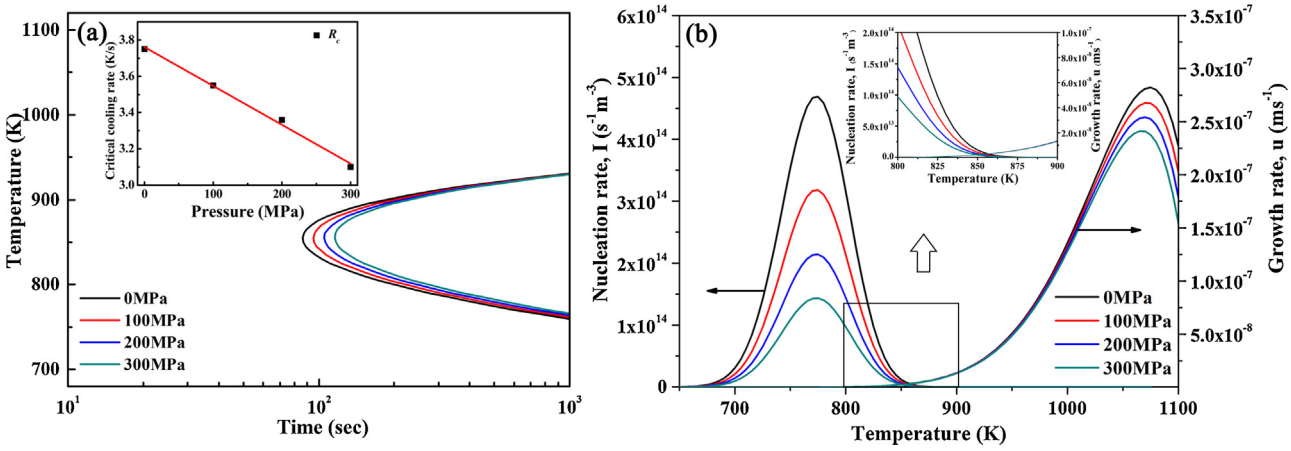

Fig. 4. (a) CCT cure under different pressure by using the modified model,insert is plots of critical cooling rates, R_c, versus pressure, (b) Nucleation rate and growth rate of $Zr_{55}Cu_{30}Al_{10}Ni_5$ under different pressure.

Table 1
Major material property and the processing parameters used in the numerical simulations.

Item	Value
Thermal conductivity (W/m/K)	$2.6 \times 10^{-2}T+1$
Viscosity (Pa·s)	exp(−5.7 + 9425(*T*-366))
Density (kg/m^3)	6830
Specific heat (kJ/kg/K)	22
Liquidus temperature (K)	1184
Solidus temperature (K)	683
Initial die temperature (K)	293
Heat transfer coefficient (HTC) between the casting and die (W·m^{-2}·K)	2000
Plunger velocity (m·s^{-1})	10

and 7.8×10^3 J/mol, respectively. Value of fraction of sites on the interface f is equal to 1 here since the alloy has relatively low entropy of fusion, i.e. $\Delta S_M^f = \Delta H_M^f/T_m < 2R_g$. Interfacial energy σ is about $0.134T_r$ J/m^2 according to the statement by Miller and Chadwick (1967). The pressure P effect on the undercooling is about 4.1×10^{-2} K/MPa according to Eq. (4). The molar volume difference between the liquid and crystalline phases, ΔV, which is decreased by about 1% after crystallization from amorphous phase, is 1.11×10^{-7} m^3/mol.

Using the above isothermal viscosity value and the measured and calculated data, the TTT curve of Zr55Y0.2 alloy can be established by using Eq. (1). As shown by the black line in Fig. 3b, the TTT curve of Zr55Y0.2 alloy displays a typical nose shape at temperature near 850 K. The critical cooling rate R_c is about 6.5 K/s, which is computed using equation $R_c \approx (T_m - T_n)/t_n$, here T_n and t_n are the temperature and time at nose point of the curve, respectively. However, Hng et al. (1996) reported that the cooling rate required to form a metallic glass by TTT curve is overestimated. A more realistic estimation of R_c is to construct a continuous cooling transformation (CCT) curve by taking into account the transformation rate at each temperature during a constant cooling treatment. As seen from the CCT curve in red color in Fig. 3b, the time to a given degree of crystallization is longer and temperature to that is lower for Zr55Y0.2 alloy during continuous cooling compared with that in the TTT curves (black line in Fig. 3b). The recalculated R_c is about 3.75 K/s (Fig. 3b), which is close to that of 1.75 K/s for Vitreloy 106a and 10 K/s for Vitreloy 106 BMG (Evenson et al., 2010).

In order to confirm the validity of result by the Uhlmann's model, the critical cooling rate of the Zr55Y0.2 is estimated directly from another method proposed by Barandiaran and Colmenero (1981), in which R_c follows the relation: $\ln(R) = ln(R_c) - \frac{b}{(T_{xc}-T_L)^2}$, here b is a constant, T_L are the liquidus temperature. The DSC curves of the alloy heated to 1373 K and then cooled at different rates are shown in Fig. 3c, exhibiting the typical endothermic peak upon melting and the exothermic peak upon solidification. It can be found that the T_{xc}, decreases with increasing of the cooling rate. The corresponding plot of $\ln(R)$ versus $1/(T_{xc} - T_L)^2$ is shown in Fig. 3d, the R_c obtained from the intercept of fitted line in Fig. 3d is determined to be 3.5 K/s, which agrees well with the R_c obtained by CCT curve (3.75 K/s from Fig. 3b). Based on the above experiment, we conclude that the calculated critical cooling rate of Zr55Y0.2 BMG is reliable and can be used to predict critical size of Zr55Y0.2 metallic glass by HPDC.

3.2.3. *Pressure effect on* R_c

In order to determine the effect of die casting pressure on R_c of Zr55Y0.2 BMG, the CCT curves under different pressures were constructed by using Eq. (5). As shown in Fig. 4a, the CCT curve shifts to the right when the pressure increases. Using the above equation, $R_c \approx (T_m - T_n)/t_n$, the critical cooling rates as function of pressure can be extracted shown as insert in Fig. 4a, the R_c for forming Zr55Y0.2 BMG is about 3.75, 3.55, 3.36 and 3.10 K/s under the pressure of 0, 100, 200 and 300 MPa, respectively. The critical cooling rate decreases monotonously with the increased pressure during die casting process. The results indicate that pressure is a beneficial factor for improving forming ability of HPDC for BMG by decreasing critical cooling rate of Zr55Y0.2. This is in good agreement with the previous results by Pan et al. (2002) and Wang et al. (2004) that high pressure can enhance the GFA through suppressing crystallization.

The intrinsic reasons of increasing GFA under pressure of die casting can be given based on the nucleation and growth behaviour of Zr55Y0.2 under different pressure. As exhibited in Fig. 4b, the pressure can reduce both the maximum for nucleation rate and growth rate of Zr55Y0.2 alloy under a deep undercooling, which is consistent with the results calculated in works by Wang et al.

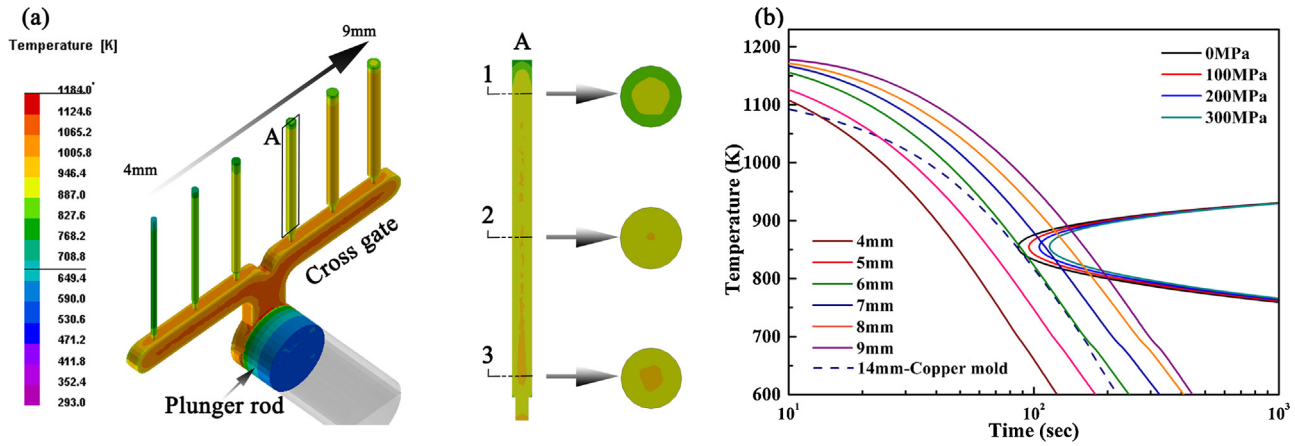

Fig. 5. (a) Cross-section of temperature field of the cylindrical casting with different diameters during solidification from different views, (b) Critical size of $Zr_{55}Cu_{30}Al_{10}Ni_5$ bulk metallic glass under different pressures during solidification. The dash line shows the cooling rate of $Zr_{55}Cu_{30}Al_{10}Ni_5$ BMG fabricated by copper mold casting.

(2004) and Han et al. (2012). As we known, the R_c of BMG is mainly determined by stability of the melt during the range of "nose" temperature. Out of this range, either the nucleation rate or growth rate is too small so that the effect of nucleation and growth behavior on critical cooling rate of BMG can be ignored. In the present case, the magnified nucleation and growth rate in "nose" temperature range, i.e. 800–900 K, is shown in the inset of Fig. 4b. The nucleation rate is obviously suppressed as the pressure increases, but the growth rate under various pressures has not significantly increased or decreased. According to model built by Uhlmann (1972), hence, the time that forms a particular volume fraction (10^{-6}) of the crystalline phase increases with the increase of pressure in "nose" temperature range. Therefore, pressure could decrease the critical cooling rate of glass formation (Fig. 4b), thus improve the forming ability of HPDC.

In general, the pressure in HPDC process would increase the nucleation rate, thus be used to refine grain of the alloy. In present case, nucleation rate decreases with increasing of pressure is ascribed the different material property at different temperature range. For traditional HPDC materials, such as aluminum alloy and magnesium alloy, the ability of undercooling is limited, crystallization would occur in the melt once the temperature of melt is 30–40 K below the solidification temperature. Actually, in this temperature range, this model also indicates that the nucleation rate increases with increasing of pressure, which has been verified by experimental and theoretical calculation results of Han et al. (2012). While for Zr55Y0.2 alloy with high GFA at the temperature near "nose", as the degree of supercooling is far larger than traditional material, the effect of pressure on decreasing the atoms diffusion ability plays a dominant role (Wang et al., 2004). As such, nucleation rate decreases with increasing of pressure, thereby leading to critical cooling rate decreases with increasing of pressures.

3.3. Critical size under different HPDC parameters

As a low-cost and time-efficient method, numerical simulation is efficient to study the solidification process and determine the cooling rate of the alloy during HPDC. The cooling rate of die casting in actual production process depends on a number of process variables such as cycle times, duration, water layout, casting geometry, as well as molten metal temperature. In order to simplify model, the cast cylindrical samples with diameters ranging from 4 mm to 9 mm were set to determine the critical size. The size of the mold was 300 × 300 × 100 mm, the casting is located at the center of the mold. The filling process is not considered here. In the numerical simulations, the mold material was H13 steel as in real die casting production line, whose properties were extracted from the ProCAST software database. The thermal conductivity is obtained from (Yamasaki et al., 2005), specific heat is achieved from (Kanomata et al., 2008), and heat transfer coefficient (HTC) between the casting and die is given by Huang et al. (2013). All the material properties of Zr55Y0.2 and processing parameters used in the simulations are shown in Table 1.

Fig. 5a displays the temperature field of the castings during solidification with casting temperature of 1184 K. As seen from the figure, the surface temperature of cylindrical castings increases with sample diameter (Fig. 5a). Meanwhile, the temperature at the position close to pouring gate (point 3) is higher than that close to top of sample (point 1) due to the heating effect of large amount of melt in cross gate (Fig. 5a). Once the minimum cooling rate in the sample is higher than critical cooling rate, the cast samples form a full amorphous structure. Therefore, the cooling rate of a sample is herein referred to the selected minimum cooling rate in the sample. The cooling curves of the castings with different diameters as well as the CCT curves for the Zr55Y0.2 alloy are shown in Fig. 5b. The cooling rate curve for the casting with 6 mm diameter is tangent to the CCT curve of the alloy under the pressure of 0 MPa. This indicates that the critical size of the Zr55Y0.2 BMG by die casting is 6 mm under 0 MPa pressure. It was also exhibited that pressure would increase the critical size but the increment is as small as about 1 mm when the pressure increases from 0 MPa to 300 MPa (Fig. 5b). Furthermore, as the dashed line shown in Fig. 5b, the critical size of purified Zr55Y0.2 BMG is determined to be 14 mm when the H13 steel mold is replaced by copper mold, whose size is smaller to critical size of high pure $Zr_{55}Cu_{30}Ni_5Al_{10}$ BMG prepared by copper mold casting by Yokoyama et al. (2007). The calculated cooling rates here seem like far smaller than that of traditional materials, such as aluminum and magnesium alloys. This is mainly ascribed to the reason as follows: on one hand, the casting temperature for present case is above 1184 K, which is far higher than that of aluminium alloy or magnesium alloy (always below 973 K). On the other hand, the cooling rate here is the minimum located at the center of sample, while the thermal conductivity of $Zr_{55}Cu_{30}Al_{10}Ni_5$ BMG (Yamasaki et al., 2005) is far smaller than that of aluminium alloy or magnesium alloy (only about 1/8), indicating the heat in the center of the sample is more difficult to be taken out, resulting a smaller cooling rate at this site. Actually, the cooling rate at the surface is as large as several hundreds K/s, suggesting that surface of sample can solidify to solid in several seconds like the traditional material.

In order to reveal the reasons why the critical size of Zr55Y0.2 BMG prepared by using copper mold is far larger than that by using

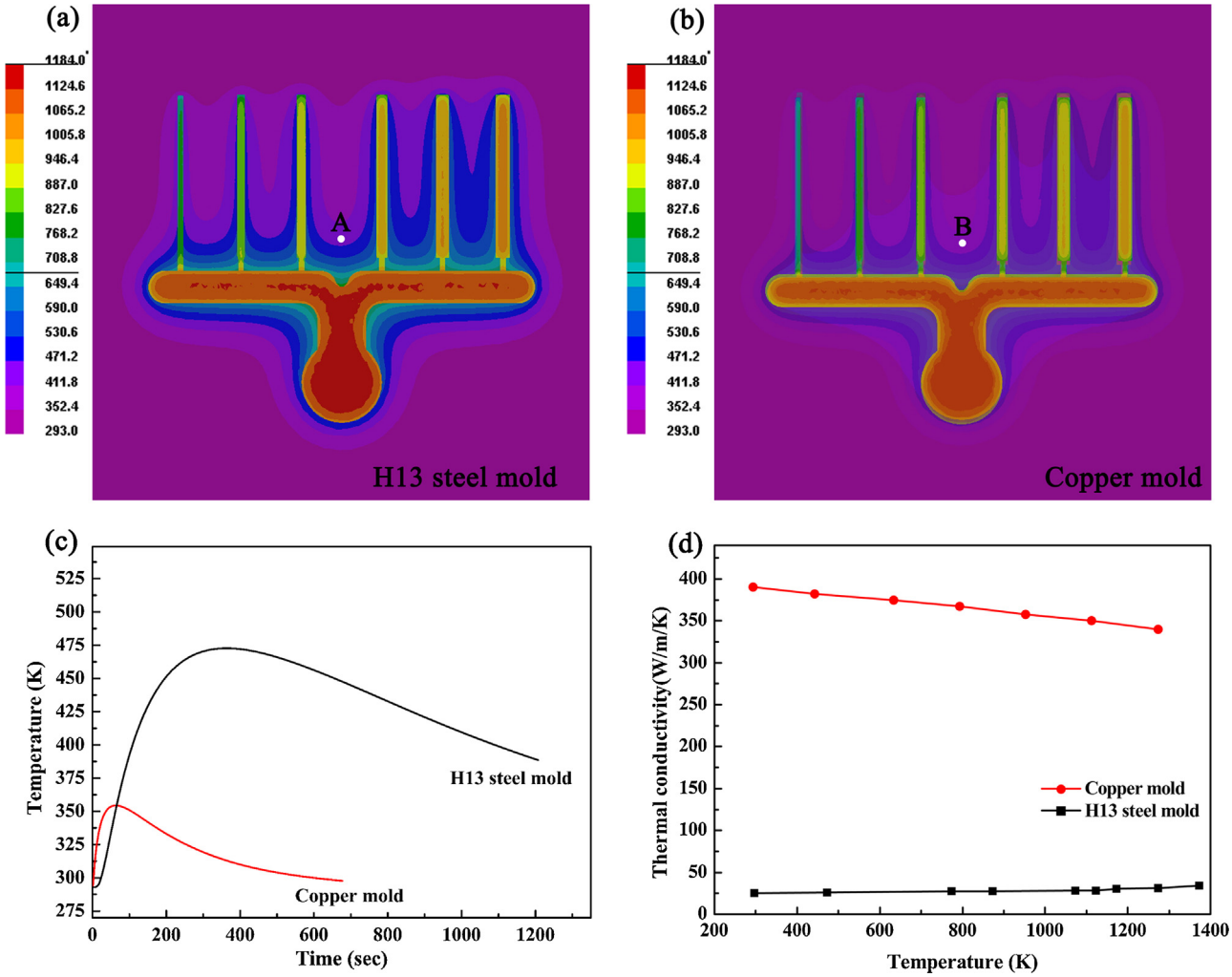

Fig. 6. Temperature field during solidification process for different mold: (a) H13 steel mold, (b) copper mold; (c) Temperature changes during solidification in H13 steel mold and copper mold (d) thermal conductivity as function of temperature for copper mold and H13 steel mold.

the H13 mold, the heat transfer process of the castings with the two different mold materials was studied. The temperature fields of the different mold during solidification are displayed in Figs. 6a–b. The average temperature of the castings by using H13 steel mold is higher than the one by using copper mold (Fig. 6a–b). Meanwhile, the temperature of H13 steel mold is higher than that of the copper mold, especially at position close to the interface of the casting and mold. The temperature variation vs time at the same position (point A and B in Fig. 6a–b) in the two different molds is displayed in Fig. 6c. As shown in Fig. 6c, the temperature in copper mold reaches quickly to the maximum of 360 K and then decreases during solidification. While for the H13 steel mold, the temperature rise rate is smaller than that of copper, but its maximum temperature (~475 K) is larger than that of copper mold. This is attributed to the difference in thermal conductivity of mold materials used. As shown in Fig. 6d, the thermal conductivity of copper is about 10 times larger than that of the H13 steel, indicating that heat in the Zr55Y0.2 melt can be much more easily taken out by the copper mold. Thus, the cooling rate of the BMG fabricated by copper mold is far larger than that by H13 steel (Shabadi et al., 2015). Another reason for Zr55Y0.2 with a smaller critical size is the heating effect of the melt in cross gate, which is essential to ensure a steady flow of metal to mold cavity and to decrease impurity content in the casting (Fig. 5a). The heating effect of the melt in the cross gate would decrease the cooling rate of the castings (Huang et al., 2013).

Based on above discussions, the critical size of Zr55Y0.2 BMG is dependent on the intrinsic critical cooling rate of the glass-forming alloy and extrinsic cooling condition of the castings. For the critical cooling rate, it is determined by the difficulty in bypassing crystallization which can be inhibited by exerting the casting pressure. For the cooling rate, it is affected not only by heat dissipating speed, i.e. thermal conductivity, but also by external heat input, i.e. casting temperature, which is also one of the most important process parameters during HPDC (Mao et al., 2010). During HPDC, the mold material generally remains unchanged. Therefore, the processing parameters, which can affect the critical size, is mainly the casting pressure and casting temperature. In order to give a guidance of the industrialized production of BMGs, the critical BMG sizes of Zr55Y0.2 BMG fabricated by HPDC under different pressure and casting temperature are calculated and demonstrated as a 3D contour figure shown in Fig. 7a. As displayed, the critical size decreases with increasing casting temperature, and the critical size decreases from 6 mm to 4 mm when the casting temperature increases from 1184 K (liquidus temperature) to 1484 K. This is agree well with Mao et al. (2010) that crystalline phases are precipitated in amorphous matrix as increasing the casting temperature is due to more heat is brought about into mold. The pressure could enhance the GFA and thus increase the critical casting size of BMG. However, the increment in critical casting size is very small, within 1 mm, under the actual production pressure of below 200 MPa (Fig. 7a). In

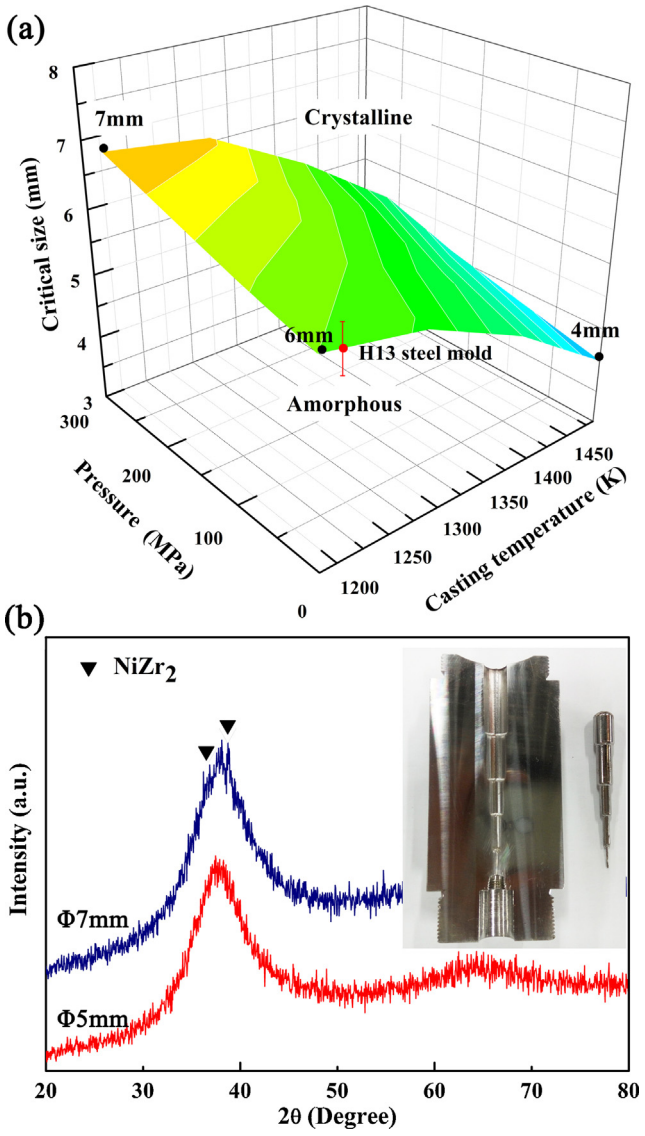

Fig. 7. (a) Critical size of $Zr_{55}Cu_{30}Al_{10}Ni_5$ BMG by die casting under different pressures and casting temperatures, (b) XRD patterns of $Zr_{55}Cu_{30}Al_{10}Ni_5$ alloys fabricated by H13 steel mold with the inset showing the H13 mold and the suction-cast specimens with 1, 3, 5, 7, and 9 mm in diameter.

order to verify the critical size of Zr55Y0.2 BMG fabricated by die casting, a casting experiment was carried out by using a stair shape H13 steel mold. The melting temperature was well controlled in the experiments by applying the arc current of 250 A on each alloy ingot for about 5 s before quenching, ensuring that the casting temperature was close to the liquidus temperature. The XRD patterns of the Zr55Y0.2 alloys display that the sample in 5 mm diameter can form a completely amorphous structure, while the $NiZr_2$-type face centered cubic (fcc) structured crystal phases form in the samples with diameters of 7 mm (Fig. 7b), which agrees well with the numerical simulation results (Fig. 7a).

The great advantage of HPDC is its capability of fabricating near-net form complex geometries components with high dimensional accuracy and less defects. Overall, the critical size of HPDC for Zr55Y0.2 BMG in the present case is large enough for some applications, such as, mobile telephone shell. The obtained results confirm that die casting is a feasible route for fabricating low cost Zr-based BMGs with suitable size for application. This work provides a guideline for designing and fabricating Zr-based BMG parts by die casting for the industrial production. It could be expected that the complex shape BMG parts fabricated by HPDC would be widely used in our daily life in the near future.

4. Conclusions

(1) Critical size of industrial grade $Zr_{55}Cu_{30}Ni_5Al_{10}$ BMG is improved by a two-step arc-melting process and adding a trace of rare earth yttrium elements.
(2) A modified model was developed to estimate the critical cooling rate of $(Zr_{55}Cu_{30}Ni_5Al_{10})_{99.8}Y_{0.2}$ bulk metallic glass by considering the casting pressure effect. Coupling the modified model and numerical simulation, the critical size of $(Zr_{55}Cu_{30}Ni_5Al_{10})_{99.8}Y_{0.2}$ BMG prepared by H13 steel mold is predicted to be 4–7 mm under different process parameters, which is successfully validated by the experimental test.
(3) A high pressure in die casting increases the critical size but the increment extent up to 1 mm. An increasing casting temperature would reduce critical size caused by more heat to dissipate. Thermal conductivity of mold plays a critical role in determining the critical size of $Zr_{55}Cu_{30}Ni_5Al_{10}$ BMG fabricated by HPDC.
(4) HPDC is a feasible route for fabrication of low cost Zr-based BMGs with suitable size for application.

Acknowledgments

P. J. Li gratefully acknowledges the financial support from the National Basic Research Program of China under contract No. 2013CB632203. Z. Y. Liu would like to thank the financial support from Natural Science Foundation of Guangdong Province (2014A030310189) and Natural Science Foundation of SZU (Grant No: 201439). L.C. Zhang is grateful for the financial support by the Australian Research Council's Discovery Projects funding (DP130103592).

References

Barandiaran, J.M., Colmenero, J., 1981. Continuous cooling approximation for the formation of a glass. J. Non-Cryst. Solids 46, 277–287.
Cheng, J.L., Chen, G., Liu, C.T., Li, Y., 2013. Innovative approach to the design of low-cost Zr-based BMG composites with good glass formation. Sci. Rep. 3, 2097.
Davies, H.A., Aucote, J., Hull, J.B., 1974. The kinetics of formation and stabilities of metallic glasses. Scr. Mater. 8, 1179–1190.
Deng, L., Zhou, B.W., Yang, H.S., Jiang, X., Jiang, B.Y., Zhang, X.G., 2015. Roles of minor rare-earth elements addition in formation and properties of Cu–Zr–Al bulk metallic glasses. J. Alloy Compd. 632, 429–434.
Evenson, Z., Gallino, I., Busch, R., 2010. The effect of cooling rates on the apparent fragility of Zr-based bulk metallic glasses. J. Appl. Phys. 107, 123529.
Han, Z., Huang, X., Luo, A.A., Sachdev, A.K., Liu, B., 2012. A quantitative model for describing crystal nucleation in pressurized solidification during squeeze casting. Scr. Mater. 66, 215–218.
Heinrich, J., Busch, R., Nonnenmacher, B., 2012. Processing of a bulk metallic glass forming alloy based on industrial grade Zr. Intermetallics 25, 1–4.
Hng, H.H., Li, Y., Ng, S.C., Ong, C.K., 1996. Critical cooling rates for glass formation in Zr-Al-Cu-Ni alloys. J. Non-Cryst. Solids 208, 127–138.
Hu, Q., Fu, M.W., Zeng, X.R., 2014. Thermostability and thermoplastic formability of $(Zr_{65}Cu_{17.5}Ni_{10}Al_{7.5})_{100-x}RE_x$ (x = 0. 25-3.25, RE Y, Gd, Tb, Dy, Ho, Er, Tm, Yb, Lu) bulk metallic glasses. Mater. Des. 64, 301–306.
Huang, X.S., Lv, Z.G., He, L.J., Mi, G.B., Li, P.J., 2013. Computer-aided designs of die and thermal control for fabrication of A356 wheels. Mater. Trans. 54, 1491–1495.
Inoue, A., Takeuchi, A., 2011. Recent development and application products of bulk glassy alloys. Acta Mater. 59, 2243–2267.
Inoue, A., Kong, F.L., Zhu, S.L., Shalaan, E., Al-Marzouki, F.M., 2015. Production methods and properties of engineering glassy alloys and composites. Intermetallics 58, 20–30.
Jiang, F., Wang, Z.J., Zhang, Z.B., Sun, J., 2005. Formation of Zr-based bulk metallic glasses from low purity materials by scandium addition. Scr. Mater. 53, 487–491.
Johnson, W.L., 1986. Thermodynamic and kinetic aspects of the crystal to glass transformation in metallic materials. Prog. Mater. Sci. 30, 81–134.
Kang, H.G., Park, E.S., Kim, W.T., Kim, D.H., 2000. Fabrication of bulk Mg-Cu-Ag-Y glassy alloy by squeeze casting. Mater. Trans. 7, 846–849.
Kanomata, T., Sato, Y., Sugawara, Y., Kimura, H.M., Kaneko, T., Inoue, A., 2008. Specific heat of Zr-based metallic glasses. J. Alloy Compd. 461, 39–41.

Liu, L.H., Yang, C., Yao, Y.G., Wang, F., Zhang, W.W., Long, Y., Li, Y.Y., 2015. Densification mechanism of Ti-based metallic glass powders during spark plasma sintering process. Intermetallics 66, 1–7.
Mao, J., Zhang, H.F., Fu, H.M., Wang, A.M., Li, H., Hu, Z.Q., 2010. Effects of casting temperature on mechanical properties of Zr-based metallic glasses. Mater. Sci. Eng. A 527, 981–985.
Miller, W.A., Chadwick, G.A., 1967. On the magnitude of the solid/liquid interfacial energy of pure metals and its relation to grain boundary melting. Acta Meter. 15, 607–614.
Pan, M.X., Yao, Y.S., Zhao, D.Q., Zhuang, Y.X., Wang, W.H., 2002. Pressure-controlled nucleation and growth in $Zr_{41}Ti_{14}Cu_{12.5}Ni_{10}Be_{22.5}$ bulk metallic glass close to and beyond glass transition temperature. Phys. Lett. A 303, 229–234.
Qiao, J.W., Jia, H., Liaw, P.K., 2016. Metallic glass matrix composites. Mater. Sci. Eng. R 100, 1–69.
Ramasamy, P., Szabo, A., Borzel, S., Eckert, J., Stoica, M., Bárdos, A., 2016. High pressure die casting of Fe-based metallic glass. Sci. Rep. 6, 35258.
Shabadi, R., Avettand-Fènoël, M.N., Simar, A., Taillard, R., Jain, P.K., Johnson, R., 2015. Thermal conductivity in yttria dispersed copper. Mater. Des. 65, 869–877.
Telford, M., 2004. The case for bulk metallic glass. Mater. Today 7, 36–43.
Turnbull, D., 1965. Phase changes. Prog. Solid State Phys. 3, 225–306.
Uhlmann, D.R., 1972. A kinetic treatment of glass formation. J. Non-Cryst. Solids 7, 337–348.
Wang, W.H., Wang, Z.X., Zhao, D.Q., Tang, M.B., Utsumi, W., Wang, X.L., 2004. High-pressure suppression of crystallization in the metallic supercooled liquid $Zr_{41}Ti_{14}Cu_{12.5}Ni_{10}Be_{22.5}$: influence of viscosity. Phys. Rev. B 70, 092203.
Yamasaki, M., Kagao, S., Kawamura, Y., 2005. Thermal diffusivity and conductivity of $Zr_{55}Al_{10}Ni_5Cu_{30}$ bulk metallic glass. Scr. Mater. 53, 63–67.
Yamasaki, T., Maeda, S., Yokoyama, Y., Okai, D., Fukami, T., Kimura, H.M., Inoue, A., 2006. Viscosity measurements of $Zr_{55}Cu_{30}Al_{10}Ni_5$ supercooled liquid alloys by using penetration viscometer under high-speed heating conditions. Intermetallics 14, 1102–1106.
Yokoyama, Y., Mund, E., Inoue, A., Schultz, L., 2007. Production of Zr55Cu30Ni5Al10 glassy alloy rod of 30 mm in diameter by a cap-cast technique. Mater. Trans. 48, 3190–3192.
Yuan, C.C., Ma, J., Xi, X.K., 2012. Understanding the correlation of plastic zone size with characteristic dimple pattern length scale on the fracture surface of a bulk metallic glass. Mater. Sci. Eng. A 532, 430–434.
Zhang, Y., Pan, M.X., Zhao, D.Q., Wang, R.J., Wang, W.H., 2000. Formation of Zr-based bulk metallic glasses from low purity of materials by yttrium addition. Mater. Trans. 11, 1410–1414.